Dynamic load analysis of the connecting bolts in a universal joint

Yuchen An[a,b], Jing Liu[a,b,*], Zengguang Li[c]

[a] Northwestern Polytechnical University, School of Marine Science and Technology, Xi'an, 710072, P. R. China
[b] Northwestern Polytechnical University, Laboratory for Unmanned Underwater Vehicle, Xi'an, 710072, P. R. China
[c] China Ship Development And Design Center, Shanghai, 201108, P. R. China

Highlights

- A flexible dynamic model of the connecting bolts is presented.

- A multibody dynamic model of the universal joint is established.

- Influence of the preload, speed and load on the bolt loads were researched.

- Advantages of the presented method were shown by comparing with the rigid models.

Abstract

Dynamic loads of the connecting bolts in a universal joint can greatly affect the bolt fatigue and fracture, as well as the machinery safety and stability. But few researches focused on those. To obtain the dynamic load characteristics of the connecting bolts in a universal joint, this paper established a flexible dynamic model for the connecting bolts. A multibody dynamic model of a universal joint is developed. The dynamic loads on the connecting bolts of the universal joint are analyzed. The influences of the preloads, speeds and loads are studied. The amplitude and frequency properties are obtained. The effect of the preload is small when the preload is in the range of 80%~120% of the standard value. The load and speed have great influence on the time- and frequency-domain dynamic loads of the bolts. The flexible dynamic model of the connecting bolt is closer to the actual situation than the rigid model since it can consider the preload and deformation of the bolts. This study can provide guidance for the fatigue life prediction of the universal shaft and its bolts.

Keywords

dynamic loads; connecting bolts; universal joint; dynamic model.

1. Introduction

The universal joint has the advantages of the wide power transmission range, simple structure, high reliability and easy to maintenance, which can transmit the torques and power in the mechanical systems. It is widely used in various ships, vehicles, power engineering and other fields [18][25]. As the components for connecting the universal joint and the input- output shafts, the connecting bolts have great influences on the safety and stability of the daily operation of the universal joint and the whole transmission system [2]. The dynamic loads can greatly affect the bolt fatigue and fracture. Thus, a study of the dynamic loads of connecting bolts on the universal joint is necessary.

Many researchers studied the loads on the connecting bolts [6]. Shi et al. [19] presented a finite element (FE) model for the connecting bolts of the flange by using the equivalent beam model. The load-stress curve of the bolt was obtained by using the FE analysis. The fatigue damage of the bolt was predicted and verified by the Palmgren-Miner linear cumulative damage theory. Weijtjens et al. [22] obtained the load transfer function for the connecting bolts of the flange in the support structure of the offshore wind power unit based on the in-situ monitoring data. The function was verified by using a FE analysis. They also studied the contributory factors for the load transfer proc-ess. Jamia et al. [5] established an equivalent reduced-order model for the flange connecting structure. Their model considered the frictions between the contact interfaces. They predicted the flange dynamic response caused by the dynamic loads from the presented model. The results were verified by using the FE analysis. Qin et al. [17] studied the influence of the bolt loosening on the time-varying stiffness of the rotating joint interface by using the nonlinear FE simulation. Sharda et al. [12] pointed out that the external load, material and geometry have great influences on the fatigue performance of the connecting bolts in the wind turbines. They presented a fatigue assessment method to estimate the bolt endurance. Nazarko et al. [16] conducted a static tensile test to obtain the elastic wave signals of the connecting bolts of the flange. It seems that the elastic wave signal was changed by the load. The forces on the bolt were recognized and predicted by using the artificial networks. Zhou et al. [29] pointed out that the small preload or large external load would lead to the yield deformation on the bolts of the flange in the wind turbine foundation. Zeng et al. [27] established a FE model for the flange connecting bolts in the combustion chamber casing of an aircraft. The stress and deformation of the connecting bolts of the flange under the axial tensile and bending load were calculated. Weiser and Corves [23] analyzed the

(*) Corresponding author.
E-mail addresses: Y. An (ORCID: 0000-0002-3478-147x): 2021100562@mail.nwpu.edu.cn, J. Liu (ORCID: 0000-0003-2323-3475): jliu@cqu.edu.cn, Z. Li (ORCID: 0000-0002-7563-0109): 22102106@qq.com

dynamics, deflection and vibration characteristics of the mechanics. The influences of the bolt connection stiffness and damping were considered. Hu et al. [4] conducted the analysis for the connecting bolts in the motor suspending of a high-speed train by using the numerical and test methods. It seems that the alternating load from the motor and cardan shaft misalignment were the main reasons for producing the bolt fatigue and fracture.

Moreover, the dynamic characteristics of the universal joint could affect the load of the connecting bolts. Venugopal et al. [21] calculated the stress and angular deflection of the universal joint in a vehicle under different working angles, torques and materials. Wu and Niu [24] analyzed the dynamic stability of the U-joint by using the monodromy matrix approach. Ma et al. [15] calculated and verified the constant velocity transmission condition based on the dynamic characteristics of the double Cardan joint. They found out the phase angle with the smallest speed fluctuation. Zhang et al. [28] formulated the interference curve between two connecting forks of the universal joint. It seems that the workspace of two connecting forks in the universal joint is a curved surface, which was affected by the geometric parameters. Guo et al. [3] analyzed the dynamic characteristics of the single cross universal joint. Bulut and Parlar [1] analyzed the dynamic stability of the elastic shaft torsional vibration in the universal shaft. They studied the effects of the misalignment angle, inertia and rigidity ratios on the torsional vibrations. Lu et al. [14] conducted a dynamic model for the universal joint considering the cross shaft neck clearance. It pointed that the small clearance could lengthen the universal joint transient duration. The large clearance could affect the output moment. Liu et al. [7] studied the relationship between the radial clearance and contact force of the universal joint under different torques by using the FE analysis. Most above works were focused on the static load, preload and fatigue damage analysis of the connecting bolts by using the FE model. Although series of studies in the field of fault and fatigue life of the bearing rotor system have been conducted by Liu and coworkers [8, 9, 10, 11, 20], but few researches studied the dynamic loads and fatigue life of the bolts in the universal joint. Therefore, to evaluate the practical load conditions and fatigue life of the universal joint and obtain the dynamic forces of the universal joint, it is necessary to research the dynamic loads by considering the bolt deformation, preload and different working conditions.

This paper presents a flexible dynamic model for the flange connecting bolts in a universal joint. A multibody dynamic (MBD) model of the shafting consisted of the universal joint, bolts and shafts is developed. The dymanic load characteristics in time- and frequency- domain can be obtained by presented model. The influences of the deformantion, preload and working condition are also investigated. A numerical calculation for the shaft under various working conditions is applied to obtain the dynamic loads of the flange bolts. The results from the rigid and flexible models of the bolts are compared. The flexible model of the bolts can consider the torsion and bending deformations of bolts, as well as the angular displacements between the adjacent flanges.

2. Dynamic modelling method

2.1. Modelling method of the connecting bolts in the universal joint

In this study, eight bolts are evenly arranged on each pair of the flange set. The diameter of the bolt distribution circle is 482 mm as shown in Fig. 1. In the previous researches about the multi-body dynamics of the connecting bolts in the universal joint, two bolt modeling methods were used, such as the rigid modelling method and flexible modelling method. In the rigid modeling method [14], the bolts, flange and shaft were regarded as the rigid bodies; the bolts and shaft were not deformed; the torque and power were totally transmitted from the input flange to output flange by the bolts. Although the rigid

modelling method has less time consumption, it cannot consider the bolt preload, collision and rebounding between the bolts and flanges. Therefore, the influences of the preload, deformation and displacement were ignored by the rigid modelling method.
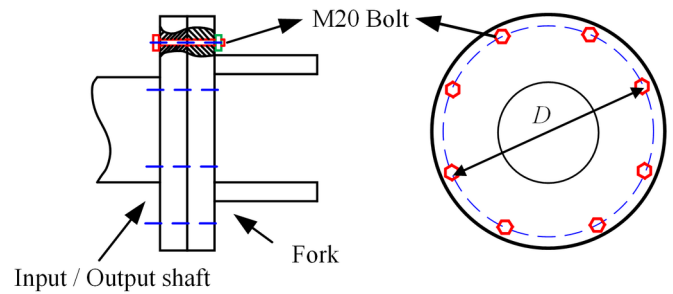

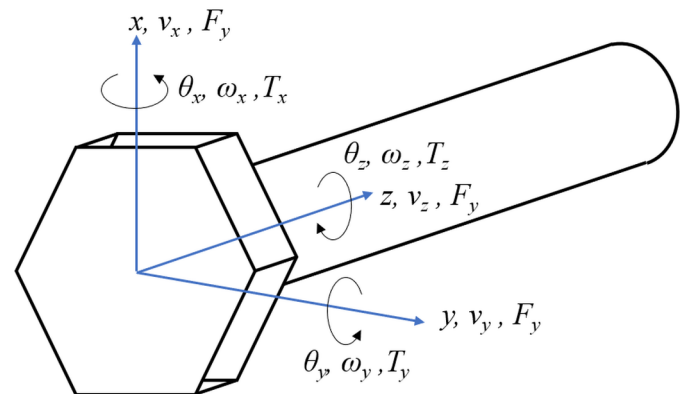Fig. 1. The bolt connection of the shaft flange in the universal joint

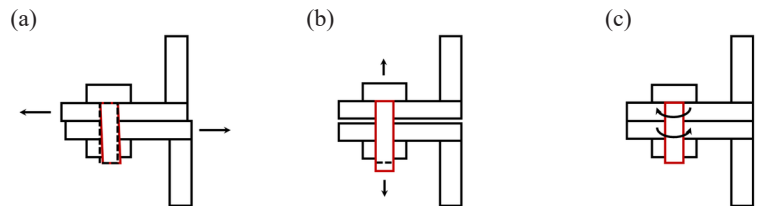Fig. 2. The flexible connection model of the bolt

Fig. 3. The bolt deformation caused by the displacement of the flange: (a) bending deformation caused by the radial displacement, (b) tensile deformation caused by the axial displacement, and (c) torsional deformation caused by the angular displacement

In the presented flexible modeling method, the bolt is regarded as a flexible body; the torque and power are transmitted through the deformation of the preloaded bolts as shown in Figs. 2 and 3. It can reflect the interaction between the bolts and flanges, which is more accurate than the rigid modelling method. Therefore, the flexible modelling method is selected to obtain the dynamic loads of the connecting bolts in this study. The dynamic equation of the bolts is described as:

$$\begin{bmatrix} F_x \\ F_y \\ F_z \\ T_x \\ T_y \\ T_z \end{bmatrix} = - \begin{bmatrix} k_{11} & 0 & 0 & 0 & 0 & 0 \\ 0 & k_{22} & 0 & 0 & 0 & 0 \\ 0 & 0 & k_{33} & 0 & 0 & 0 \\ 0 & 0 & 0 & k_{44} & 0 & 0 \\ 0 & 0 & 0 & 0 & k_{55} & 0 \\ 0 & 0 & 0 & 0 & 0 & k_{66} \end{bmatrix} \cdot \begin{bmatrix} x \\ y \\ z \\ \theta_x \\ \theta_y \\ \theta_z \end{bmatrix} - \begin{bmatrix} c_{11} & 0 & 0 & 0 & 0 & 0 \\ 0 & c_{22} & 0 & 0 & 0 & 0 \\ 0 & 0 & c_{33} & 0 & 0 & 0 \\ 0 & 0 & 0 & c_{44} & 0 & 0 \\ 0 & 0 & 0 & 0 & c_{55} & 0 \\ 0 & 0 & 0 & 0 & 0 & c_{66} \end{bmatrix} \cdot \begin{bmatrix} v_x \\ v_y \\ v_z \\ \omega_x \\ \omega_y \\ \omega_z \end{bmatrix} + \begin{bmatrix} F_1 \\ F_2 \\ F_3 \\ T_{b1} \\ T_{b2} \\ T_{b3} \end{bmatrix}$$

(1)

where F_x, F_y, F_z, T_x, T_y and T_z are the forces and torques on the bolt in x, y and z directions; k_{11}, k_{22} and k_{33} are the stiffness coefficients in the translational directions of the bolts; k_{44}, k_{55} and k_{66} are the stiffness coefficients in the rotational directions of the bolts; x, y and z

are the translational displacements of the adjacent flanges, which also represent the tensile or bending deformation of the bolts; θ_x, θ_y and θ_z are the angular displacements of the adjacent flanges, which also represent the torsional deformation of the bolts; c_{11}, c_{22} and c_{33} are the damping coefficients of the bolts in the translational directions; c_{44}, c_{55} and c_{66} are the damping coefficients of the bolts in the rotational directions; v_x, v_y and v_z are the relative velocities of the adjacent flanges in the translational directions; ω_x, ω_y and ω_z are the relative angular velocities of the adjacent flanges in the rotational directions; F_1, F_2 and F_3 are the preload forces on the bolts in the translational directions; T_{b1}, T_{b2} and T_{b3} are the preload torques on the bolts in the rotational directions. The dynamic model of the bolt is determined by the stiffness and damping coefficients, preload force and preload torque as shown in Eq. (1). The preload force could be obtained by querying the standard value data according to the bolt type and grade, z direction is defined as the axial direction, the preload forces $F_1=F_2=0$, the preload force F_3 is 31900N (the bolt type is M20 and the grade is 3.6). The bolts are not torqued after tightening, the preload torque $T_{b1}=T_{b2}=T_{b3}=0$.

By treating the bolts as a cylinder with the uniform mass, the stiffness coefficients in the translation and rotation directions could be obtained by the material mechanics. Therefore, the translational stiffness coefficients in the circumferential direction k_{11} and k_{22}, the translational stiffness coefficient in the axial direction k_{33}, the rotational stiffness coefficients in the horizontal and vertical circumferential directions k_{44} and k_{55}, and the rotational stiffness coefficient in the axial direction k_{66} could be calculated by:

$$k_{11} = k_{22} = \frac{GA}{l} \tag{2}$$

$$k_{33} = \frac{EA}{l} \tag{3}$$

$$k_{44} = k_{55} = \frac{E}{l} = \frac{E\pi d^4}{64l} \tag{4}$$

$$k_{66} = \frac{G\pi r^4}{2l} \tag{5}$$

where E is the elastic module of the bolt material; A is the cross-section area of the bolt, which can be obtained from the corresponding technological standards; l is the length of bolt; d is the diameter of the bolt; G is the shear module of the bolt material; r is the bolt radius; I is the rotational inertia about the axial direction of the bolt. The corresponding values are shown in Table 1. The stiffness coefficients of the bolt are calculated by Eqs. (2) to (5). According to the bolt material properties, the damping coefficients in the translational and rotational directions of the bolt $c_{11}=c_{22}=c_{33}=50$ Ns/mm, $c_{44}=c_{55}=c_{66}=50$ Nmm·s/deg.

Table 1. *Properities of the connecting bolt (M20) in the universal joint*

E	G	A	l	d
200 GPa	80 GPa	314 mm^2	100 mm	20 mm

Therefore, the dynamic equation of the connecting bolt in the universal shaft in the flexible model can be written as:

$$\begin{bmatrix} F_x \\ F_y \\ F_z \\ T_x \\ T_y \\ T_z \end{bmatrix} = - \begin{bmatrix} 1.96 \times 10^{11} x \\ 1.96 \times 10^{11} y \\ 4.9 \times 10^{11} z \\ 9 \times 10^{8} \theta_x \\ 9 \times 10^{8} \theta_y \\ 7.2 \times 10^{8} \theta_z \end{bmatrix} - \begin{bmatrix} 50 v_x \\ 50 v_y \\ 50 v_z \\ 50 \omega_x \\ 50 \omega_y \\ 50 \omega_z \end{bmatrix} + \begin{bmatrix} 0 \\ 0 \\ 31900 \\ 0 \\ 0 \\ 0 \end{bmatrix} \tag{6}$$

2.2. A multibody dynamic model of the universal shaft

The relative motions of the components of the studied universal shaft are shown in Fig. 4. Here, T_1 is the input torque of the shaft; T_2 is the load of the shaft; ω_1 and ω_3 are the rotating speed of the input and output shaft; β_1 is the acute angle between the input shaft and intermediate shaft; β_2 is the acute angle between the intermediate shaft and output shaft; γ is the angle along the rotation direction between the plane formed by the input-intermediate shafts and that formed by the intermediate-output shafts; φ is the angle between the forks at the input and output sides of the intermediate shaft; θ_1 and θ_3 are the rotation angles of the input and output shafts; θ_{21} and θ_{22} are the phase angles of the fork at the input and output sides of the intermediate shaft.
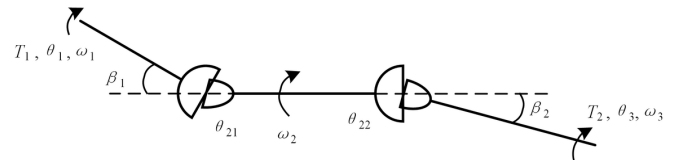

Fig. 4. Motion of the universal shafting

According to the geometric relationship of the universal joint at the input side of the shaft, it has:

$$\frac{\tan \theta_1}{\tan \theta_{21}} = \frac{1}{\cos \beta_1} \tag{7}$$

Then, θ_{21} can be written as:

$$\tan \theta_{21} = \tan \theta_1 \cos \beta_1 \tag{8}$$

$$\theta_{21} = \tan^{-1}(\tan \theta_1 \cos \beta_1) \tag{9}$$

Taking the derivation of t on two sides of Eq. (9), it has:

$$\omega_2 = \frac{d\theta_{21}}{dt} = \frac{\cos \beta_1}{1 - \sin^2 \beta_1 \cos^2 \theta_1} \frac{d\theta_1}{dt} = \frac{\cos \beta_1}{1 - \sin^2 \beta_1 \cos^2 \theta_1} \omega_1 \tag{10}$$

The transmission ratio from the input shaft to intermediate shaft is obtained:

$$i_{12} = \frac{\omega_2}{\omega_1} = \frac{\cos \beta_1}{1 - \sin^2 \beta_1 \cos^2 \theta_1} \tag{11}$$

The angle relationship of the universal joint in the output side of the shaft can be obtained by:

$$\frac{\tan \theta_{22}}{\tan \theta_3} = \cos \beta_2 \tag{12}$$

$$\theta_3 = \tan^{-1}(\frac{\tan\theta_{22}}{\tan\beta_2}) \tag{13}$$

Taking the derivation of t on the two sides of Eq. (13), it has:

$$\omega_3 = \frac{d\theta_3}{dt} = \frac{\cos\beta_2}{1 - \sin^2\beta_2 \cos^2\theta_{22}} \frac{d\theta_{22}}{dt} = \frac{\cos\beta_2}{1 - \sin^2\beta_2 \cos^2\theta_{22}} \omega_2 \tag{14}$$

The relationship between the phase angle θ_{21} and θ_{22} is given by:

$$\theta_{22} = \theta_{21} - \gamma + \varphi \tag{15}$$

Then, Eq. (14) can be written as:

$$\omega_3 = \frac{\cos\beta_2}{1 - \sin^2\beta_2 \cos^2[\tan^{-1}(\tan\theta_1 \cos\beta_1) - \gamma + \varphi]} \omega_2 \tag{16}$$

The transmission ratio from the intermediate shaft to the output shaft is expressed as:

$$i_{23} = \frac{\omega_3}{\omega_2} = \frac{\cos\beta_2}{1 - \sin^2\beta_2 \cos^2[\tan^{-1}(\tan\theta_1 \cos\beta_1) - \gamma + \varphi]} \tag{17}$$

According to Eqs. (11) and (17), the transmission ratio from the input shaft to the output shaft is written as:

$$i_{13} = i_{12} \cdot i_{23} = \frac{\cos\beta_1}{1 - \sin^2\beta_1 \cos^2\theta_1} \cdot \frac{\cos\beta_2}{1 - \sin^2\beta_2 \cos^2[\tan^{-1}(\tan\theta_1 \cos\beta_1) - \gamma + \varphi]} \tag{18}$$

The shafts are coplanar in this study. The angle β_1 between the adjacent shafts is 1.95°. The phase difference between the forks is 0. The transmission ratio of the universal shafting is given by

$$i_{13} = i_{12} \cdot i_{23} = \frac{\cos\beta_1}{1 - \sin^2\beta_1 \cos^2\theta_1} \cdot \frac{\cos\beta_1}{1 - \sin^2\beta_1 \cos^2[\tan^{-1}(\tan\theta_1 \cos\beta_1)]} \tag{19}$$

By using a commercial software Adams, a MBD model of the universal shaft is proposed to conduct the numerical calculations as shown in Fig. 5. The dynamic model of the flange bolt is shown in Fig. 6. Here, F_a is the axial load of the flange bolt, F_c is the circumferential load of the bolt. The motion relationship between the components in the model can be described by various motion pairs. The input and output shafts are constrained by the cylindrical joints. The cross shafts and forks are connected by the hook's joints. The forks and input or output shaft are connected by the bolts, which are modeled by flexible method. The friction forces are considered by using the contact pairs established in the model. The static friction coefficient is 0.3, the dynaimc friction coefficient is 0.1.
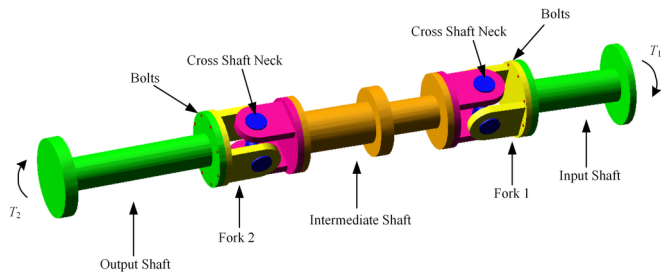

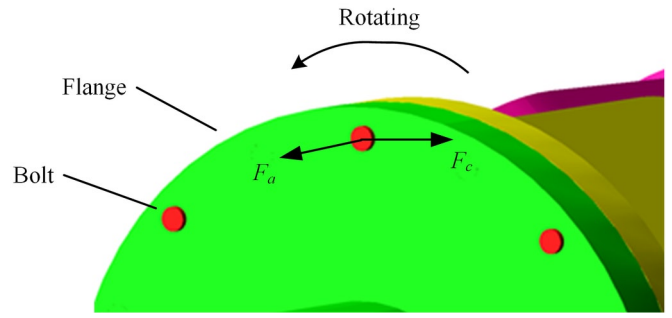Fig. 5. A multi-body dynamic model of the universal shafting

Fig. 6. The flexible bolt in the multi-body dynamic model

3. Results analysis

The influences of the shaft speeds, loads and preloads on the dynamic loads of the connecting bolts in the axial and circumferential directions are obtained. The results from the flexible model and the rigid model are compared.

3.1. Influence of the preload on the bolt dynamic loads

Figures 7 to 10 show the waveforms of the circumferential and axial dynamic loads of the bolts under different shaft speeds, loads and preloads. The speeds are 400 rpm, 600 rpm, 800 rpm and 1000 rpm. The loads are 0 kNm, 10 kNm, 20 kNm, 30 kNm, 40 kNm and 50 kNm. The preloads are 80%, 100% and 120% of the standard value (whose value is 31900 N). Figures 11 to 14 show the corresponding RMS values. The waveforms of the dynamic loads of the flange bolts are periodical ones. The frequencies of the waveforms are influenced by the rotating speed. The average values of the axial loads are almost 0. The amplitudes of the axial loads increase with the shaft load. The amplitudes of the axial loads of the output flange are higher than those of the input flange. The average values and amplitudes of the circumferential loads varies with the shaft load and rotating speed. The average values of the circumferential loads of the output flange are lower than those of the input flange.

In Figs. 11 to 14, the RMS values of the circumferential loads varies from 0.9 kN to 20.1 kN for the studied shaft load cases. The RMS values of the axial loads of the input flange bolts varies from 1.3 kN to 1.7 kN for the studied shaft load cases. The RMS values of the axial loads of the output flange almost are fixed at 1.4 kN. The RMS values of the circumferential loads of the input flange bolts are lower than those of the output flange bolts. The waveforms and RMS values of the circumferential and axial loads under different preloads are identical ones. The preload variation has small influences on the dynamic loads of the bolts, when it varies from 80% to 120% standard value. Thus, the following analysis will use the standard preload.

3.2. Circumferential loads on the bolts

3.2.1. Circumferential loads on the input flange bolts

Figures 15(a) and (b), 16(a) and (b) show the waveforms and spectra of the circumferential loads of the input flange bolt under different shaft speed and load conditions. When the shaft is unloaded, the loads are consisted of the basic to tripling frequencies. The basic frequency amplitudes vary from 8.6 N to 52.5 N with the shaft speed. The doubling frequency amplitudes vary from 6.1 N to 48.9 N with the shaft speed. The tripling frequency amplitudes vary from 9.9 N to 59.2 N with the shaft speed. When the shaft is full-loaded, the loads consist of the basic frequency and few doubling frequencies. The basic frequency amplitude varies from 714.4 N to 956.3 N with the speed.

Figure 17 shows the effects of the load and shaft speed on the circumferential load of the input flange bolts. The corresponding data is depicted in Table 2. When the shaft is loaded, the circumferential load of the input flange bolt is affected by the shaft load. The maxi-
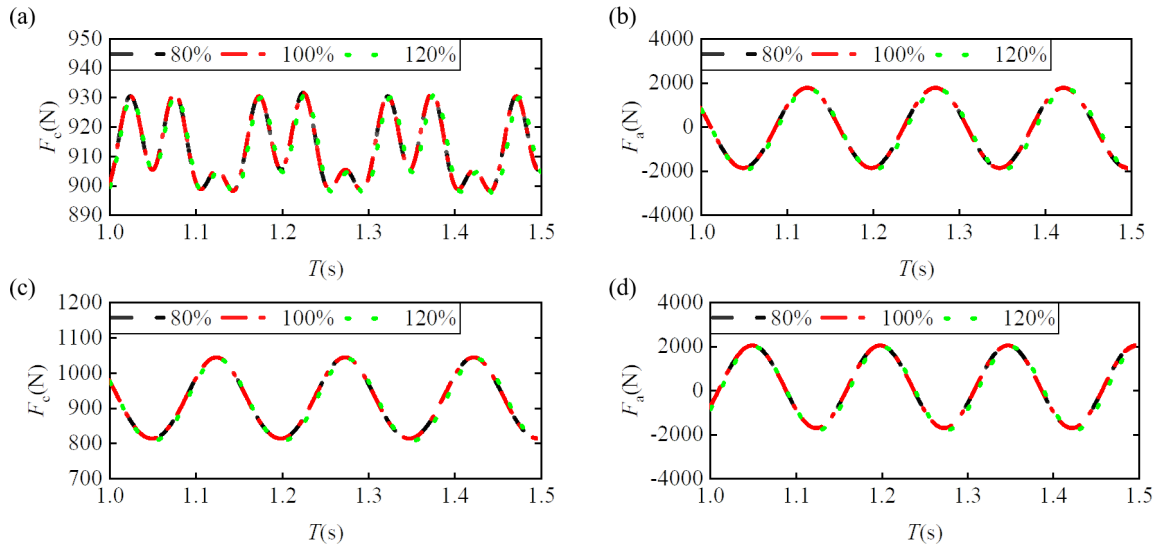
Fig. 7. The time-domain dynamic loads on the bolts with different preloads under 400 rpm and 0 kNm: (a) circumferential loads of the input flange bolts, (b) axial loads of the input flange bolts, (c) circumferential loads of the output flange bolts, and (d) axial loads of the output flange bolts
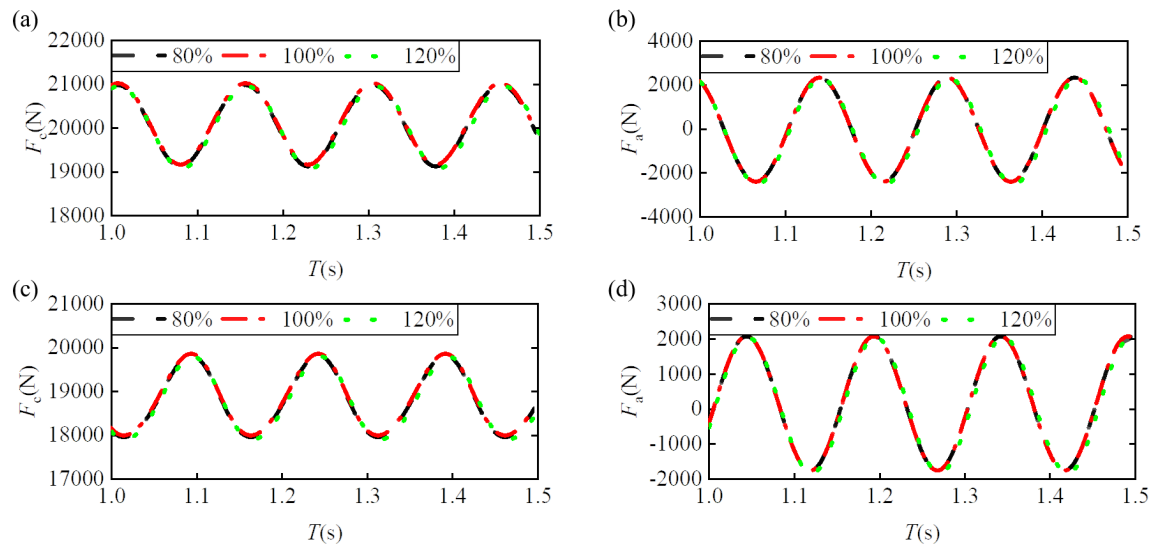

Fig. 8. The time-domain dynamic loads on the bolts with different preloads under 400 rpm and 50 kNm: (a) circumferential loads of the input flange bolts, (b) axial loads of the input flange bolts, (c) circumferential loads of the output flange bolts, and (d) axial loads of the output flange bolts
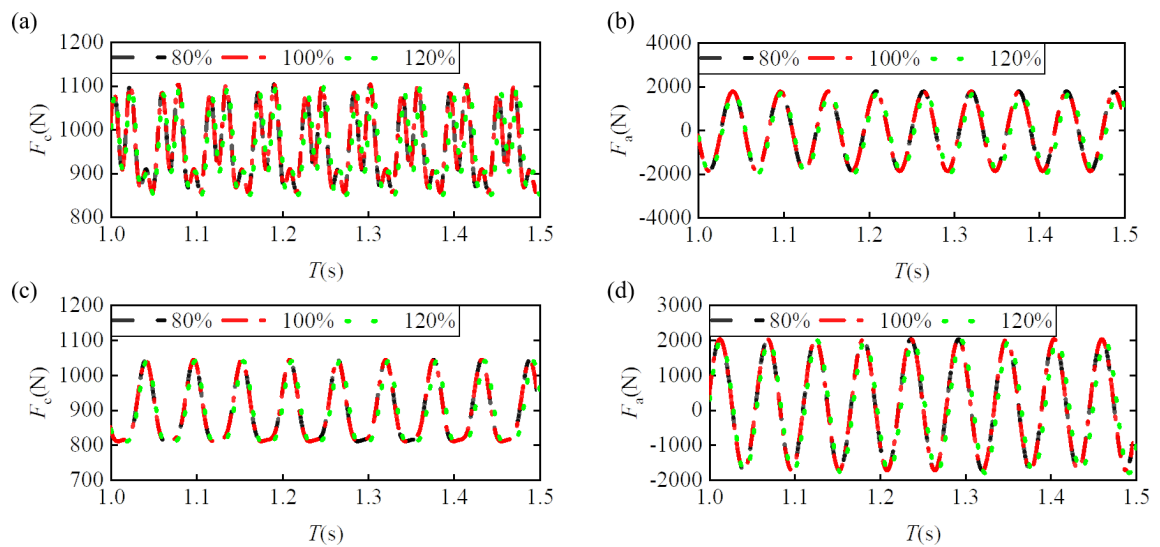

Fig. 9. The time-domain dynamic loads on the bolts with different preloads under 1000 rpm and 0 kNm: (a) circumferential loads of the input flange bolts, (b) axial loads of the input flange bolts, (c) circumferential loads of the output flange bolts, and (d) axial loads of the output flange bolts
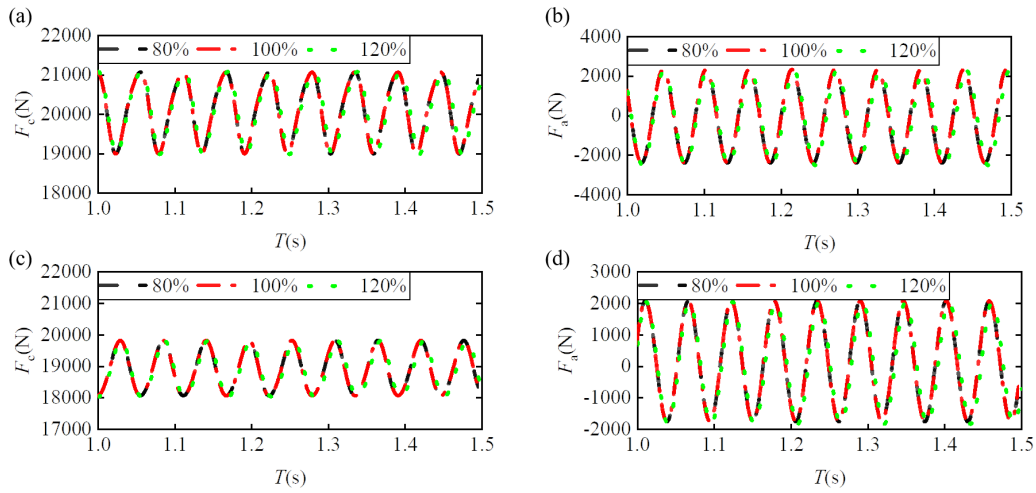
Fig. 10. The time-domain dynamic loads on the bolts with different preloads under 1000 rpm and 50 kNm: (a) circumferential loads of the input flange bolts, (b) axial loads of the input flange bolts, (c) circumferential loads of the output flange bolts, and (d) axial loads of the output flange bolts
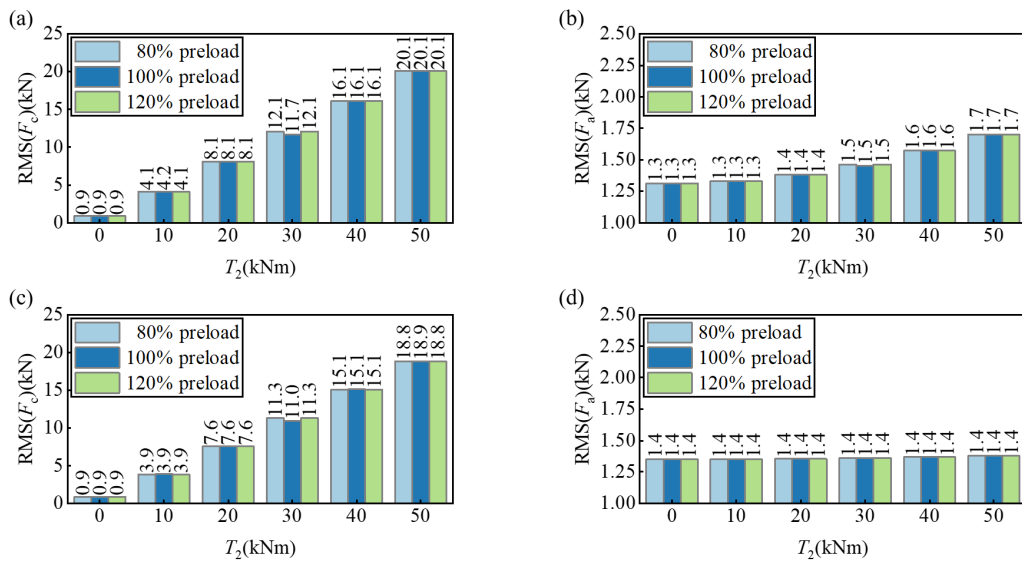

Fig. 11. The RMS value of the dynamic loads of the bolt with different preloads under 400 rpm and different loads: (a) RMS value of circumferential loads on the bolts in input flange, (b) RMS value of axial loads on the bolts in input flange, (c) RMS value of circumferential loads on bolts in output flange, and (d) RMS value of axial loads on the bolts in output flange
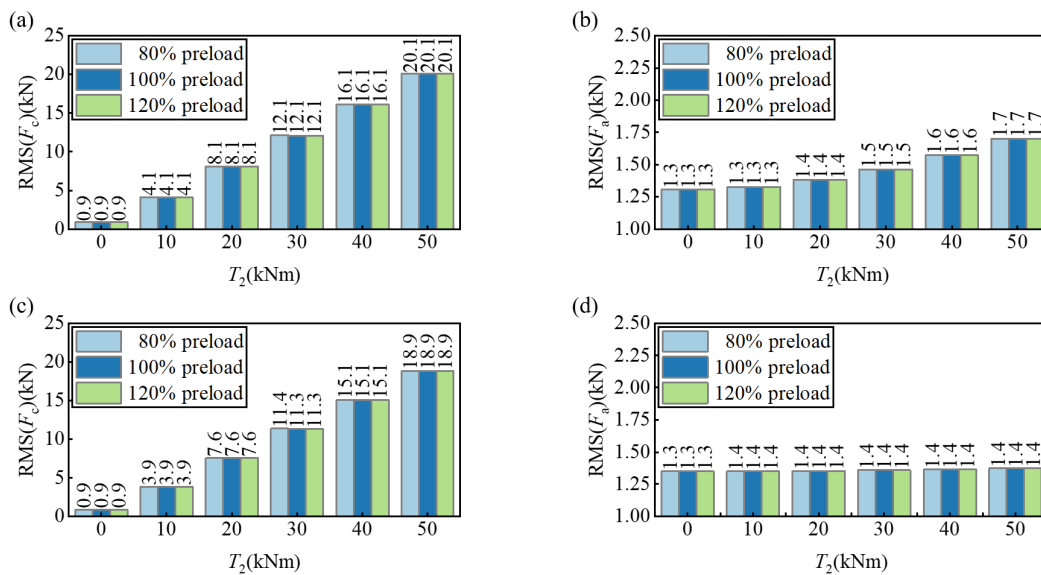

Fig. 12. The RMS value of the dynamic loads of the bolt with different preloads under 600 rpm and different loads: (a) RMS value of circumferential loads on the bolts in input flange, (b) RMS value of axial loads on the bolts in input flange, (c) RMS value of circumferential loads on bolts in output flange, and (d) RMS value of axial loads on the bolts in output flange

Fig. 13. *The RMS value of the dynamic loads of the bolt with different preloads under 800 rpm and different loads: (a) RMS value of circumferential loads on the bolts in input flange, (b) RMS value of axial loads on the bolts in input flange, (c) RMS value of circumferential loads on bolts in output flange, and (d) RMS value of axial loads on the bolts in output flange*
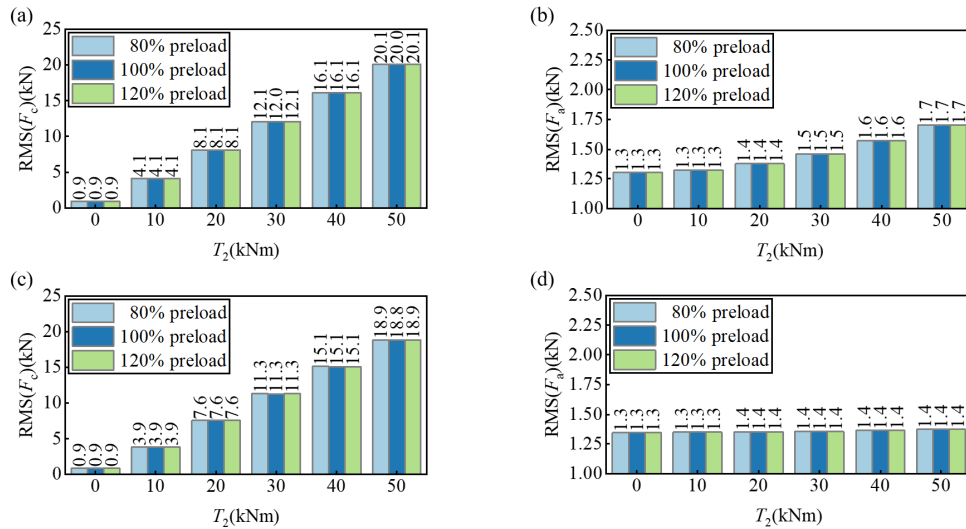

Fig. 14. *The RMS value of the dynamic loads of the bolt with different preloads under 1000 rpm and different loads: (a) RMS value of circumferential loads on the bolts in input flange, (b) RMS value of axial loads on the bolts in input flange, (c) RMS value of circumferential loads on bolts in output flange, and (d) RMS value of axial loads on the bolts in output flange*
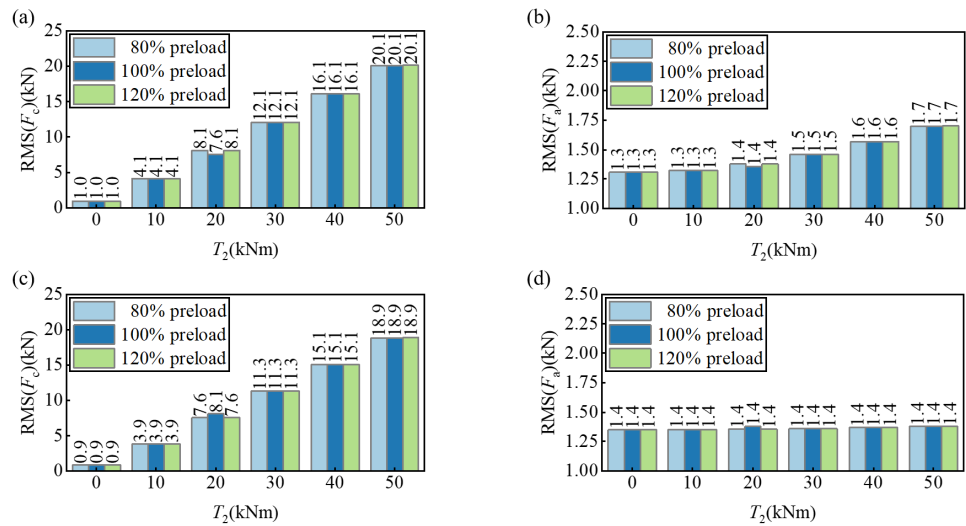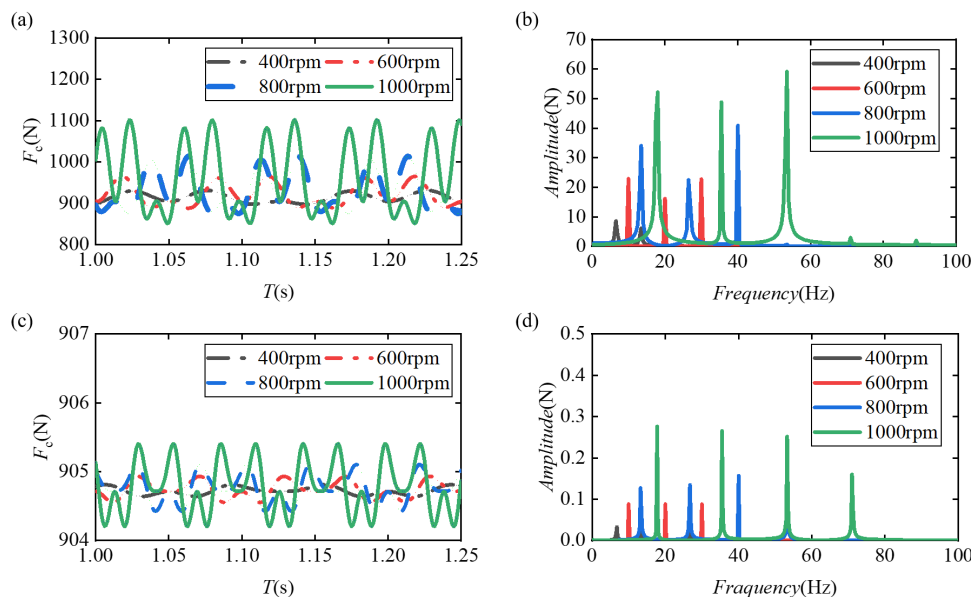

Fig. 15. *The waveforms and spectra of circumferential loads on input flange bolts under no-load working condition through flexible and rigid model: (a) waveforms of flexible model, (b) spectra of flexible model, (c) waveforms of rigid model, and (d) spectra of rigid model*

Table 2. The average values and amplitudes of frequency components of the circumferential loads on the input flange bolts (N)

| Loads (kNm)	Values	Speeds			
		400 rpm	600 rpm	800 rpm	1000 rpm
0	Average	911.7	921.2	935.0	959.0
	Basic frequency amplitude	8.6	22.9	34.1	52.3
	Doubling frequency amplitude	6.1	16.2	22.5	48.9
	Tripling frequency amplitude	9.9	22.7	40.9	59.2
10	Average	4105.8	4064.8	4064.0	4057.7
	Basic frequency amplitude	739.0	930.5	808.7	699.4
	Doubling frequency amplitude	44.45	70.5	90.5	162.8
20	Average	8054.7	8052.8	8051.8	8045.4
	Basic frequency amplitude	744.7	937.5	814.5	703.8
	Doubling frequency amplitude	36.55	53.2	81.6	152.5
30	Average	11659.7	12057.9	12016.5	12050.3
	Basic frequency amplitude	748.6	942.1	818.4	706.6
	Doubling frequency amplitude	35.8	48.8	79.4	149.6
40	Average	16110.9	16067.2	16065.8	16059.5
	Basic frequency amplitude	754.4	948.5	818.2	709.9
	Doubling frequency amplitude	35.45	47.1	79.3	148.3
50	Average	20082.7	20078.4	20036.2	20070.4
	Basic frequency amplitude	760.9	956.3	829.2	714.4
	Doubling frequency amplitude	35.4	46.5	77.9	147.7
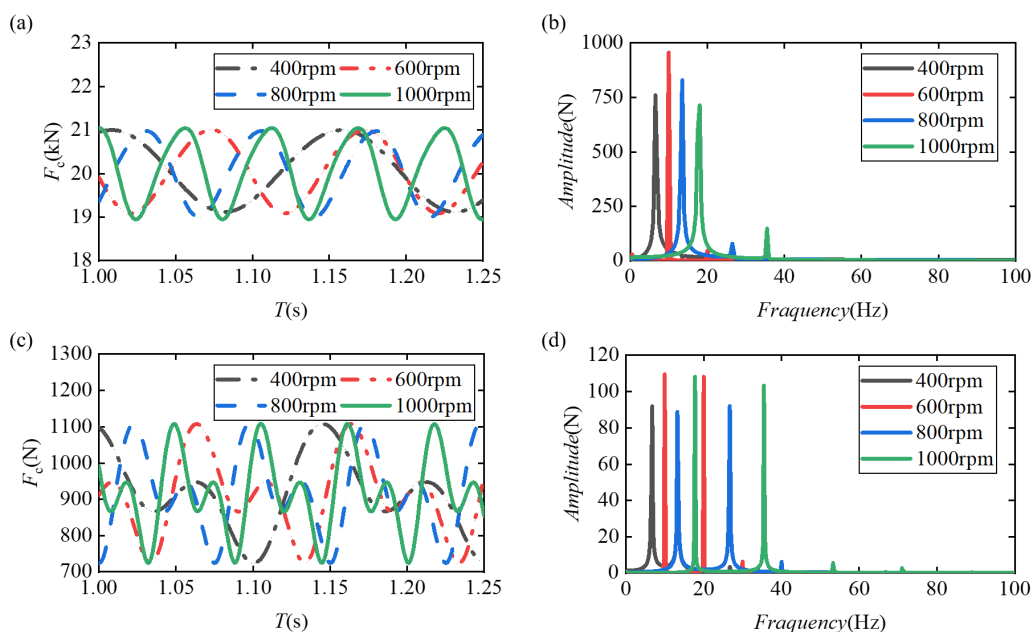
Fig. 16. The waveforms and spectra of circumferential loads on the input flange bolts under full load working condition through flexible and rigid model: (a) waveforms of flexible model, (b) spectra of flexible model, (c) waveforms of rigid model, and (d) spectra of rigid model

mum basic frequency amplitude occurs when the load is 50 kNm and the rotating speed is 600 rpm, which is 956.3 N. The average values of waveforms are unchanged with the rotating speed. The doubling frequency amplitude increase with the rotating speed. The maximum doubling frequency amplitude occurs when the load is 10 kNm and the rotating speed is 1000 rpm, which is 162.8 N.

Figures 15(c), 15(d), 16(c) and 16(d) show the waveforms and spectra of the circumferential loads of the input flange bolts of the rigid model. When the shaft is unloaded, the circumferential loads of

the input flange bolts from the flexible model are higher than those from the rigid model. The loads of the rigid model are consisted of the basic to quadrupling frequency. The amplitudes of the frequency components of the rigid model are smaller than 0.3N. When the shaft is fully loaded, the loads of the rigid model are consisted of the basic frequency and doubling frequency with the similar amplitude in the range of 80 N to 110 N.
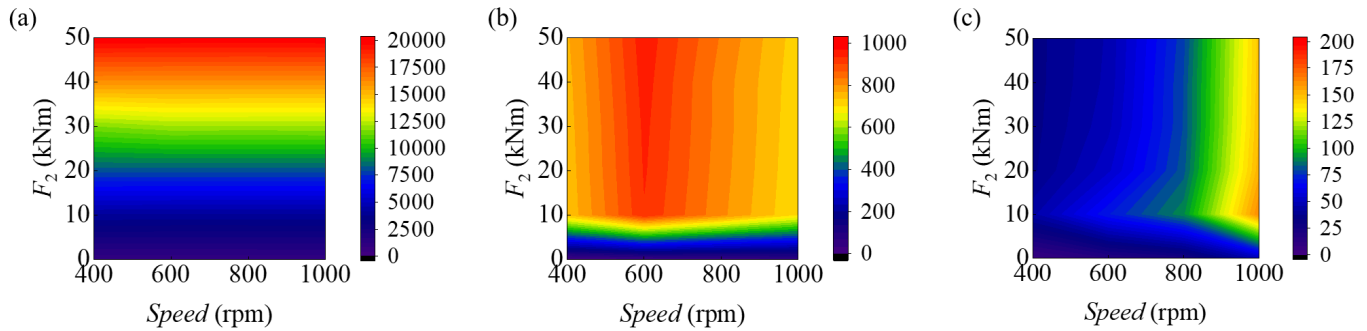
Fig. 17. *Influences of the speed and load on average, basic and doubling frequency amplitudes of the input flange bolts: (a) average value, (b) basic frequency, and (c) doubling frequency*

3.2.2. Circumferential loads on the output flange bolts

Figures 18(a) and (b), 19(a) and (b) show the waveforms and spectra of the circumferential loads of the output flange bolts under different shaft speeds and loads. When the shafting is unloaded, the loads of the flexible model are consisted of the basic frequency. The basic frequency amplitude varies from 81.8 N to 116.8 N. When the shaft is fully loaded, the loads of the flexible model are consisted of the basic frequency. The basic frequency amplitude varies from 620.9 N to 929.8 N.

Figure 20 shows the influences of the load and shaft speed on the circumferential load of the output flange bolts. The corresponding values are shown in Table 3. The circumferential loads of the output flange are influenced by the shaft speed and load. The loads are consisted of the basic frequency and small amount of the doubling frequency. The average values of the circumferential loads of the output flange bolts are influenced by the load. The maximum of the average value at the highest shaft speed and load, whose value is 18857.2 N. The basic frequency amplitudes firstly increase and then decreases with the rotating speed. The maximum basic frequency amplitude occurs when the shaft speed and load are 600 rpm and 50 kNm, whose value is 929.8 N. The doubling frequency amplitude is influenced by the load and the shaft speed. The doubling frequency amplitude firstly

decreases and then increases when the load is fixed. The maximum doubling frequency amplitude occurs when the speed and load are 400 rpm and 10 kNm, whose value is 84.2 N.

Figures 18(c) and (d), 19(c) and (d) show the waveforms and spectra of the circumferential loads of the output flange bolts of the rigid model. When the shaft is unloaded, the loads of the rigid model are consisted of the basic to the quadrupling frequency. The amplitudes of the frequency components are smaller than 1 N. When shaft is fully loaded, the loads of the rigid model are consisted of the basic and doubling frequencies with the similar amplitudes. The amplitudes of the basic and doubling frequencies of the rigid model varies from 75 to 110 N with the shaft speed.

According to the above analysis, the characteristics of the circumferential loads of the input flange bolts are similar with those of the output flange bolts. The loads of the flexible model have simpler frequency components and higher amplitudes. The loads of the rigid model are opposite. The reason of the differences between the two models is that in the presented flexible model, bending and torsional deformation occurred in the bolts when the shaft is working as shown in Figs. 3(a) and (c). The forces and torques are transmitted between the adjacent flanges through the bolt deformations. The radial and angular displacements between the adjacent flanges are also constrained by the bolts. The circumferential force caused by the displacements would act on the bolts. Therefore, in the flexible model, the average values and amplitudes of the circumferential load vary with the load and shaft speed. In the rigid model, the bolts and adjacent flanges have no defamation and displacement. The circumferential loads of the bolts are smaller than the flexible model. Moreover, the adjacent bolts and flange will rebound due to their impact interactions; and this process may cause the complex frequency components. When the shaft is loaded, the rebounding is inhibited, the frequency components become simpler as shown in Figs. 18(b) and (d), 19(b) and (d).

Table 3. *The average values and amplitudes of frequency components of the circumferential loads on output flange bolts (N)*

| Loads (kNm)	Values	Speeds			
		400 rpm	600 rpm	800 rpm	1000 rpm
0	Average	922.4	914.1	904.8	891.4
	Basic frequency amplitude	97.2	116.8	97.15	81.8
	Doubling frequency amplitude	5.5	10.5	14.3	31.7
10	Average	3864.5	3825.6	3824.6	3831.3
	Basic frequency amplitude	737.8	898.3	745.9	597.8
	Doubling frequency amplitude	84.2	76.1	51.7	67.6
20	Average	7567.1	7564.9	7563.8	7570.6
	Basic frequency amplitude	744.5	906.5	752.6	603.6
	Doubling frequency amplitude	75.8	60.9	38.3	55.2
30	Average	10950.3	11323.4	11284.5	11328.9
	Basic frequency amplitude	749.1	912.8	757.6	608.2
	Doubling frequency amplitude	74.7	58.9	37.6	55.5
40	Average	15128.2	15086.8	15084.8	15092.1
	Basic frequency amplitude	755.9	920.2	759.2	613.9
	Doubling frequency amplitude	74.8	59.7	36.9	58.1
50	Average	18856.6	18852.1	18812.3	18857.2
	Basic frequency amplitude	763.8	929.8	771.8	620.9
	Doubling frequency amplitude	75.7	61.5	38.2	61.7
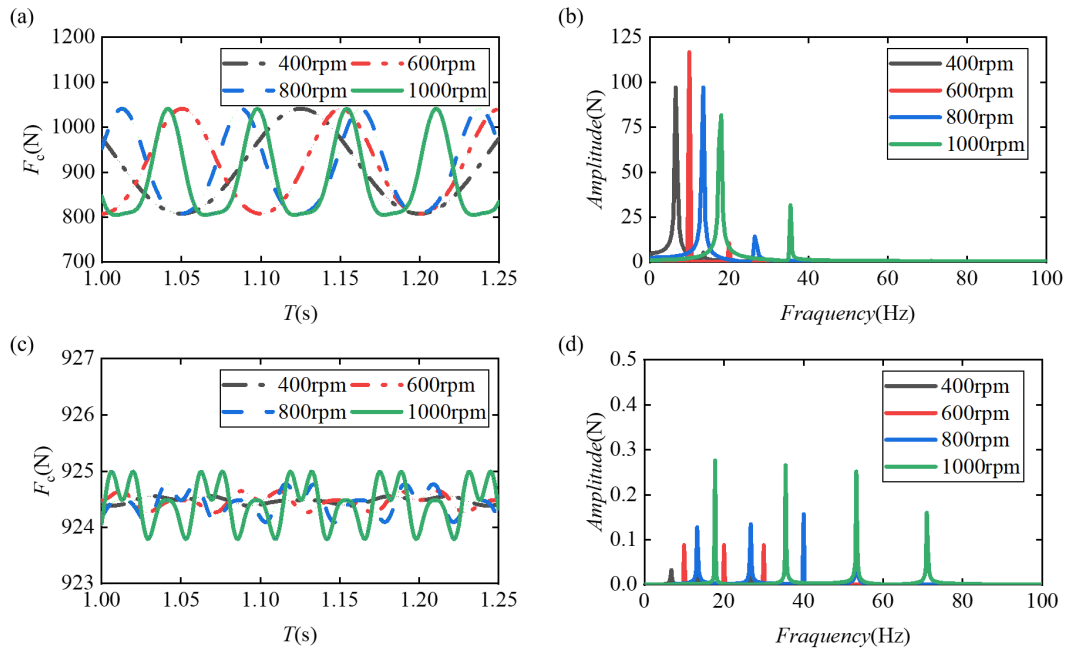
Fig. 18. *The waveforms and spectra of the circumferential loads on the output flange bolts under the unload working condition from the flexible and rigid models: (a) waveforms of flexible model, (b) spectra of flexible model, (c) waveforms of rigid model, and (d) spectra of rigid model*

Fig. 19. *The waveforms and spectra of the circumferential loads on the output flange bolts under the full load working condition from the flexible and rigid models: (a) waveforms of flexible model, (b) spectra of flexible model, (c) waveforms of rigid model, and (d) spectra of rigid model*
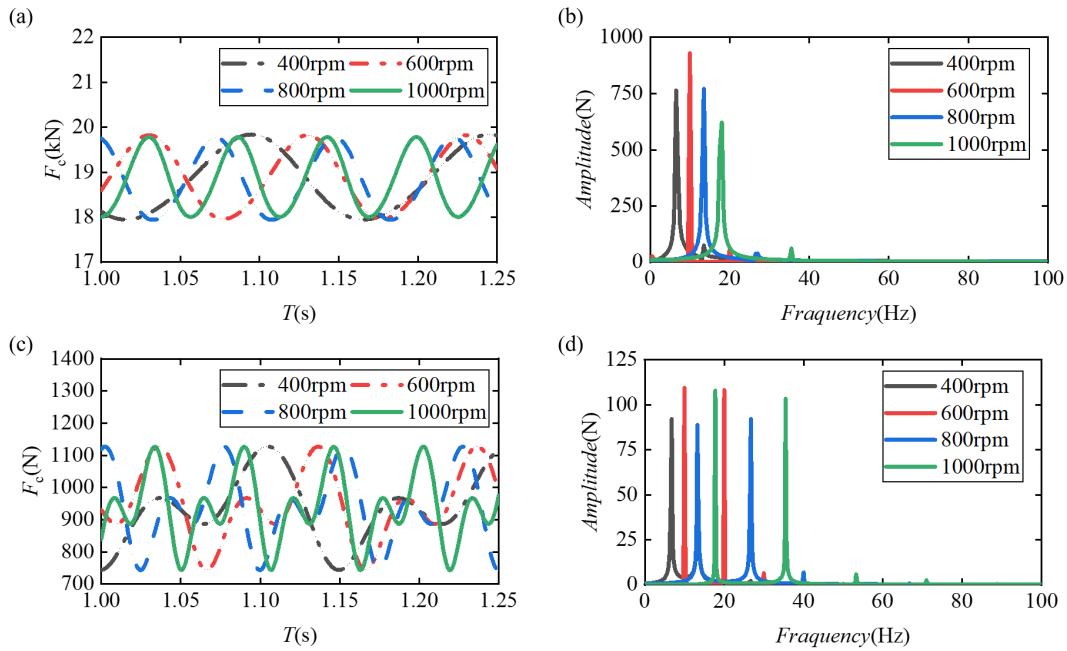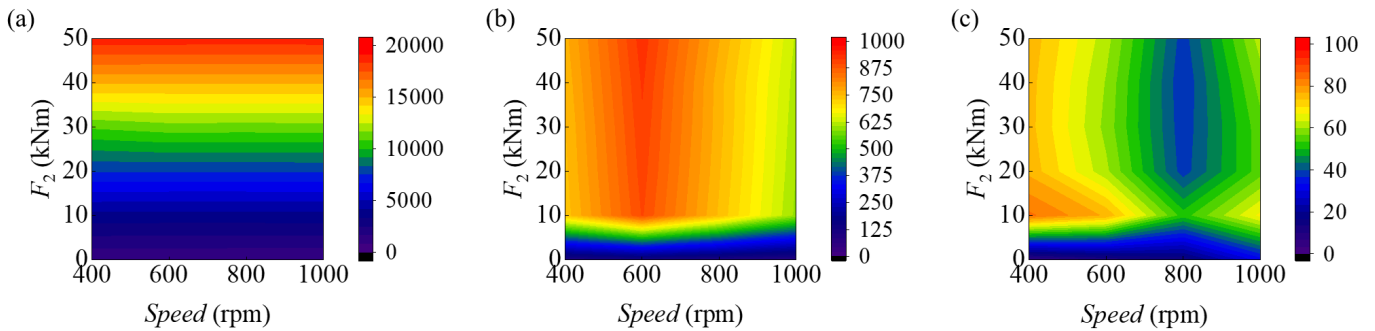

Fig. 20. *Influences of the speed and load on the average, basic and doubling frequency amplitudes of the output flange bolts: (a) average value, (b) basic frequency, and (c) doubling frequency*

3.3. Axial loads on the bolts

3.3.1. Axial loads on the input flange bolts

Figures 21(a) and (b), 22(a) and (b) show the waveforms and spectra of the axial loads of the input flange bolts under different shaft speed and load conditions. The loads are consisted of the basic frequency. When the shaft is unloaded, the amplitude of the basic frequency varies from 1292.2 N to 1846.4 N. When the shaft is fully loaded, the amplitude of the basic frequency varies from 1671.6 N to 2403.2 N.

frequency varies from 1292.2 N to 2403.2 N. The maximum basic frequency amplitude occurs at 600 rpm and 50 kNm.

Figures 21(c) and (d), 22(c) and (d) show the waveforms and spectra of the axial loads of the input flange bolts of the rigid model. When the shaft is unloaded, the loads of the rigid model are consisted of basic to the quadrupling frequency. The average values of the axial loads are 108.25 N. The amplitudes of the frequency components are smaller than 0.03 N. When the shaft is fully loaded, the average value of the loads is 110 N. The amplitudes of the frequency components vary from 5.4 N to 6.7 N.

3.3.2. Axial load on the output flange bolts

Figures 24(a) and (b), 25(a) and (b) show the waveforms and spectra of the axial loads of the output flange bolts under different shaft and load conditions. The loads are consisted of the basic frequency. When the shaft is unloaded, the amplitude of the basic frequency varies from 1334.7 N to 1903.3 N. When the shaft is fully loaded, the amplitude of the basic frequency varies from 1363.9 N to 1940.8 N. The average value of the loads varies from 67.9 N to 127.9 N.

Table 4. The average value and amplitude of the frequency components of the axial loads on input flange bolts (N)

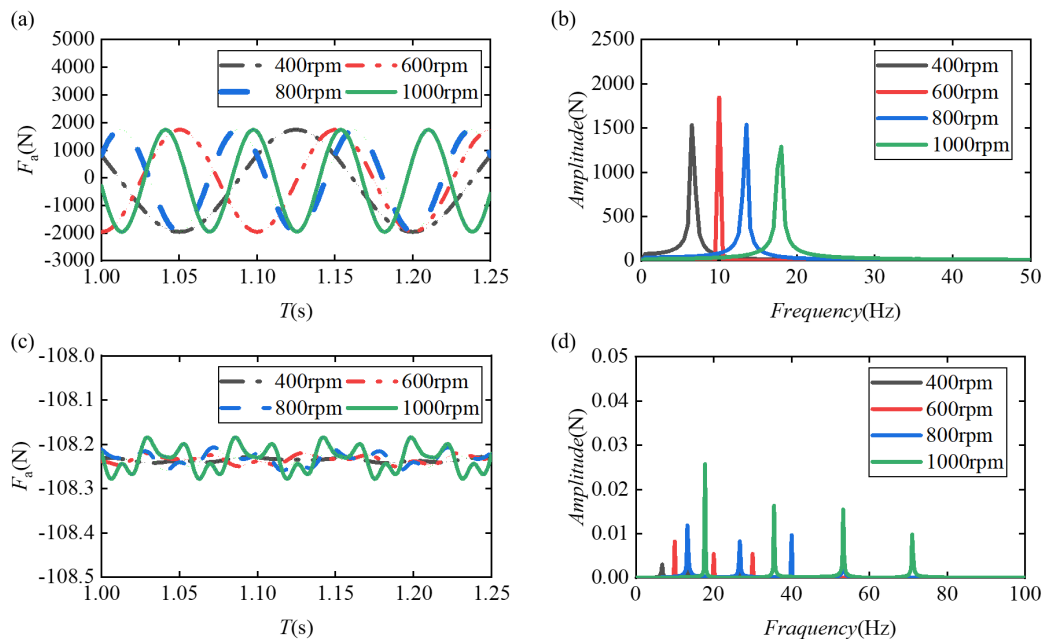| Loads (kNm)	Values	Speeds			
		400 rpm	600 rpm	800 rpm	1000 rpm
0	Average	69.1	107.4	124.6	113.9
	Basic frequency amplitude	1534.9	1846.4	1540.3	1292.2
10	Average	69.1	107.9	124.6	116.1
	Basic frequency amplitude	1555.5	1871.8	1562.1	1307.4
20	Average	69.1	107.9	124.6	118.4
	Basic frequency amplitude	1613.8	1946.2	1625.7	1356.9
30	Average	69.1	107.9	124.6	120.6
	Basic frequency amplitude	1696.5	2064.1	1725.5	1437.5
40	Average	69.1	107.9	124.5	122.8
	Basic frequency amplitude	1831.4	2218.8	1847.6	1543.9
50	Average	69.1	107.4	124.6	124.9
	Basic frequency amplitude	1976.8	2403.2	2014.5	1671.6

Fig. 21. The waveforms and spectra of the axial loads on the input flange bolts under the unload working condition from the flexible and rigid models: (a) waveforms of flexible model, (b) spectra of flexible model, (c) waveforms of rigid model, and (d) spectra of rigid model

Figure 23 shows the influences of the shaft rotating speed and load on the axial loads of the input flange bolts. Table 4 shows the corresponding data. The axial loads on the input flange bolts are influenced by the load and shaft speed. The average values increase with the shaft speed. The average value obtained by the flexible model varies from 69.1 N to 124.9 N. The maximum average value occurs when the shaft speed and load are 1000 rpm and 50 kNm. The amplitude of the basic

Figure 26 demonstrates the influences of the shaft speed and load on the axial loads of the output flange bolts. Table 5 shows the corresponding values. The average value and basic frequency amplitude are influenced by the shaft speed. The average value firstly increases and then decreases with the increment of the speed. The maximum average value occurs at 600 rpm and 40 kNm, whose value is 127.9 N. The maximum basic frequency amplitude firstly increases and then decreases with the increment of the speed. The maximum basic fre-
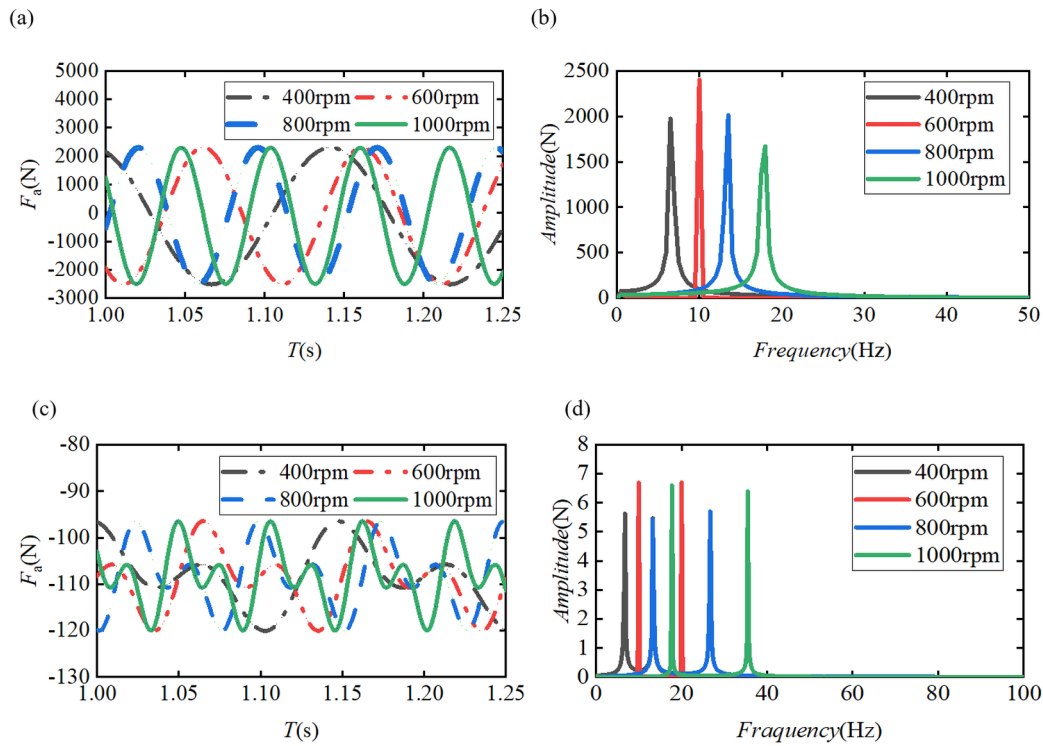
Fig. 22. The waveforms and spectra of the axial loads on the input flange bolts under the full load working condition from the flexible and rigid models: (a) waveforms of flexible model, (b) spectra of flexible model, (c) waveforms of rigid model, and (d) spectra of rigid model
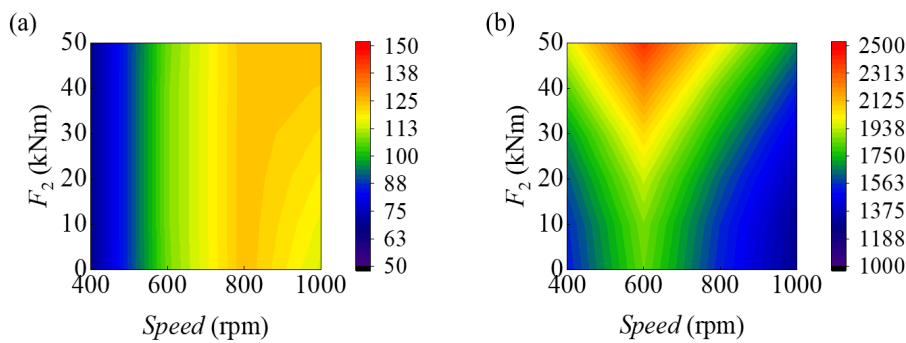

Fig. 23. Influences of the speed and load on the average, basic frequency amplitudes of the input flange bolts: (a) average value and (b) basic frequency

Table 5. The average value and amplitude of the frequency components of the axial loads on output flange bolts (N)

Loads (kNm)	Values	Speeds			
		400 rpm	600 rpm	800 rpm	1000 rpm
0	Average	67.9	108.4	127.6	119.1
	Basic frequency amplitude	1581.5	1903.3	1588.9	1334.7
10	Average	67.9	108.9	127.6	118.6
	Basic frequency amplitude	1582.7	1904.9	1590.2	1336.4
20	Average	67.9	108.9	127.6	118.1
	Basic frequency amplitude	1586.3	1909.4	1594.1	1340.2
30	Average	67.9	108.9	127.6	117.5
	Basic frequency amplitude	1591.5	1916.9	1600.4	1346.0
40	Average	67.9	108.9	127.9	116.9
	Basic frequency amplitude	1600.6	1927.4	1598.9	1353.9
50	Average	67.9	108.4	127.6	116.4
	Basic frequency amplitude	1611.0	1940.8	1620.8	1363.9

quency amplitude occurs at 600 rpm and 50 kNm, whose value is 1940.8 N.

Figures 24(c) and (d), 25(c) and (d) show the waveforms and spectra of the axial loads of the output flange bolts of the rigid model. The average value of the rigid model varies from 100 N to 110 N. When the shaft is unloaded, the loads of the rigid model are consisted of the basic to the quadrupling frequency. The frequency component amplitudes vary from 0 N to 0.5 N. When the shaft is fully loaded, the loads of the rigid model are consisted of the basic and doubling frequencies. The amplitudes vary from 5 N to 7 N.

The differences between the axial loads of the flexible model and those of the rigid model are observed. The reason is that the preload can affect the axial loads in the flexible model. The axial displacement between the adjacent flanges is constrained by the bolts. The axial force from the displacement would act on the bolts. In the rigid model, the influences of the preloads are ignored. The adjacent flanges will rebound due to their impact interactions. Then, the complex frequency components occur in the axial loads of the bolts. The rebounding is inhibited when the shaft is loaded, the tripling and quadrupling frequencies disappeared as shown in Figs. 24(b) and (d), 25(b) and (d).
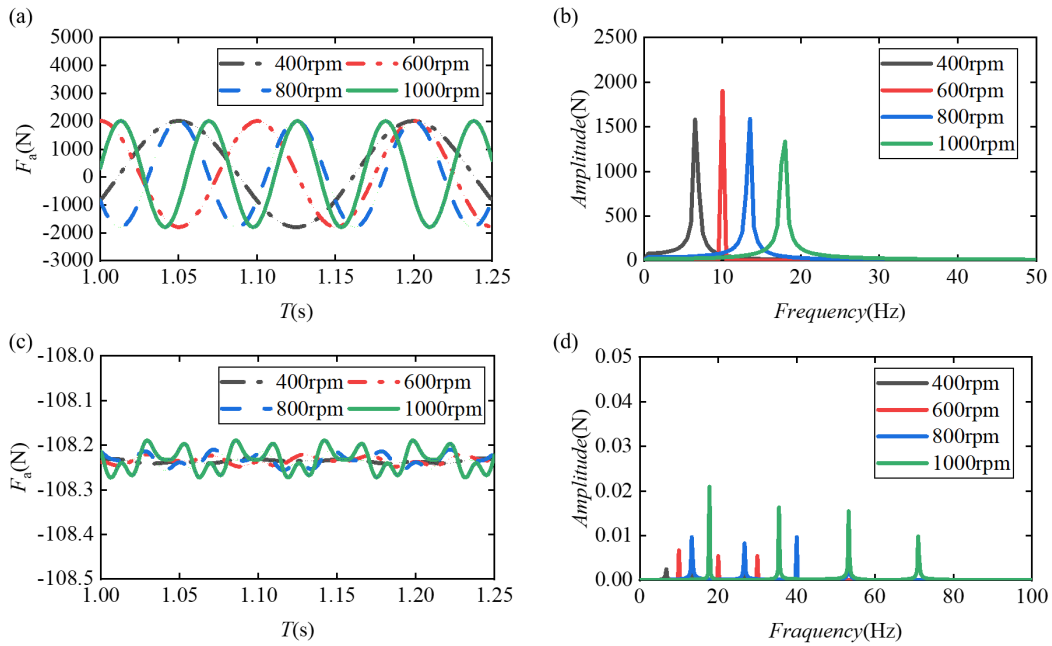
Fig. 24. The waveforms and spectra of the axial loads on the output flange bolts under the unload working condition from the flexible and rigid models: (a) waveforms of flexible model, (b) spectra of flexible model, (c) waveforms of rigid model, and (d) spectra of rigid model
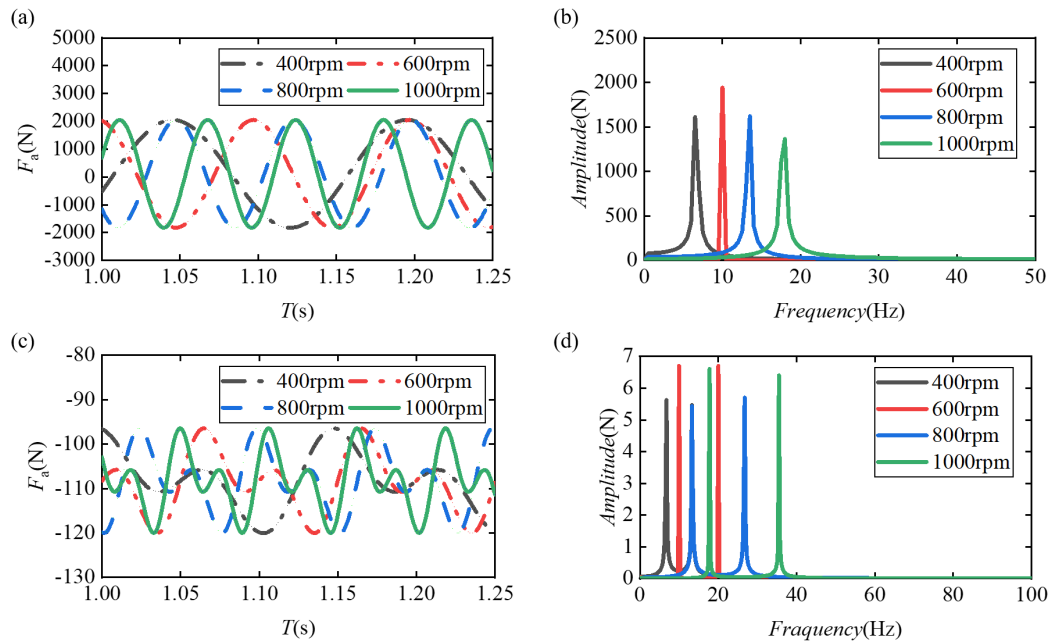

Fig. 25. The waveforms and spectra of the axial loads on the output flange bolts under the full load working condition from the flexible and rigid models: (a) waveforms of flexible model, (b) spectra of flexible model, (c) waveforms of rigid model, and (d) spectra of rigid model
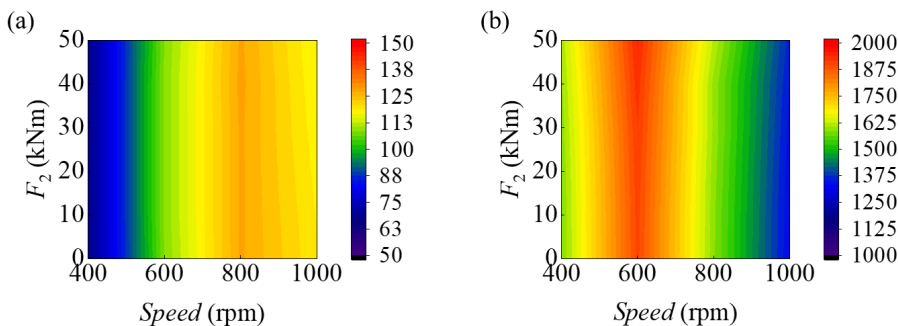

Fig. 26. Influences of the speed and load on the average, basic frequency amplitudes of the output flange bolts: (a) average value and (b) basic frequency

4. Model validation

The calculation is conducted by using the empirical method. The results from the flexible model are verified with those from the empirical method and the rigid model. The axial load of the flange bolt equals to the preload force of the bolt. The circumferential loads of the flange bolt can be expressed as [7, 13, 14, 26]:

$$F_c = \frac{2T_2}{nD} \qquad (20)$$

where, n is the bolt number of the flange connection, D is the diameter of the bolt distribution circle.

Figure 27 shows the RMS values of the circumferential loads of the input flange bolt by using the three methods. Table 6 shows the corresponding data. The differences between the loads of the three methods are observed. The results from the empirical method are higher than those from the numerical calculation by using the flexible model. Although the empirical method considers the influences of the flange parameters and the shaft working conditions. But the influences of the preload, stiffness and damping on the loads of the bolts are ignored. The more accurate values cannot be obtained by the empirical method. Thus, the flexible model can reach more accurate values than the empirical method and the rigid model.
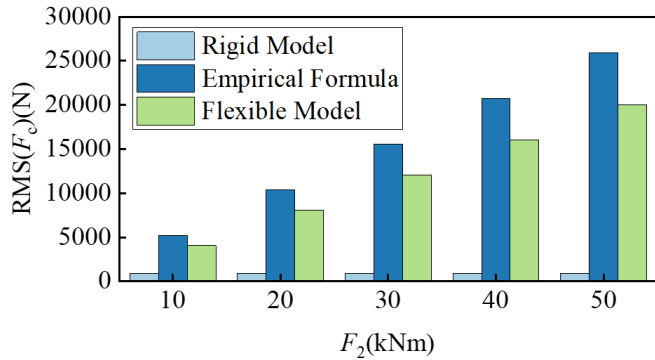

Fig. 27. The RMS values of the circumferential loads of the input flange bolts at 1000 rpm and different loads

Table 6. The RMS values of the circumferential loads on the input flange bolts by using the flexible model and the empirical method

Loads (kNm)	Rigid model (N)	Empirical method (N)	Flexible model(N)
10	905.3	5186.7	4057.65
20	906.9	10373.45	8045.4
30	909.5	15560.15	12050.3
40	913.15	20746.9	16059.45
50	917.85	25933.6	20070.35

5. Conclusions

This study presents a flexible modelling method for the connecting bolts of the universal joint. A numerical analysis for the dynamic loads of the connecting bolts is conducted. Some obtained conclusions are as follows.

(1) The presented model for the connecting bolts of the universal shaft considers the affective factors for the dynamic loads of the bolts, such as the bolt preload, deformation, damping coefficient and adjacent flanges' displacement. The presented method is close to the real situation of the bolts than those from the rigid model.

(2) When the preload on the connecting bolts of the universal joint is from 80%~120% of the standard value, it has small effect on the dynamic loads of the bolts.

(3) The average value and the basic frequency amplitude of the circumferential load are affected by the rotating speed. The double frequency amplitude is affected by the load and speed. The average value and basic frequency amplitude of the axial load are affected by the shaft rotating speed too.

(4) Based on the above analysis, the effects of the load and speed on the dynamic forces can be obtained. Then, the evaluation of the working status and fatigue life of the universal shafting can be conducted, which can provide information for the design, applications and maintenance of the universal shafting.

(5) This study only investigated the dynamic forces under the static load and rotating speed, the dynamic forces under the dynamic working condition are not studied. Furthermore, only the bolts were treated as the flexible bodies in this paper. Future research will be focused on the dynamic forces under the dynamic working condition by treating the whole universal shafting as flexible bodies.

References

1. Bulut G, Parlar Z. Dynamic stability of a shaft system connected through a Hooke's joint. Mechanism and Machine Theory, 2011, 46(11): 1689-1695, https://doi.org/10.1016/j.mechmachtheory.2011.06.012.
2. Burek R, Wydrzyński D, Sęp J, Więckowski W. The effect of tool wear on the quality of lap joints between 7075 T6 aluminum alloy sheet metal created with the FSW method. Eksploatacja i Niezawodnosc – Maintenance and Reliability 2018, 20(1): 100–106, http://dx.doi.org/10.17531/ein.2018.1.13.
3. Guo Y Y, Sun Z H, Sun Z H. The kinematics analysis on single cross universal joint. 2008 IEEE Vehicle Power and Propulsion Conference. IEEE, 2008: 1-3, https://doi.org/10.1109/VPPC.2008.4677771.
4. Hu Y, Tan A C, Liang C, et al. Failure analysis of fractured motor bolts in high-speed train due to cardan shaft misalignment. Engineering Failure Analysis, 2021, 122: 105246, https://doi.org/10.1016/j.engfailanal.2021.105246.
5. Jamia N, Jalali H, Taghipour J, et al. An equivalent model of a nonlinear bolted flange joint. Mechanical Systems and Signal Processing, 2021, 153: 25-26, https://doi.org/10.1016/j.ymssp.2020.107507.
6. Kaneda S, Tsuji H. Application of plastic region tightening bolt to flange joint assembly. ASME Pressure Vessels and Piping Conference. 2006, 47535: 255-261, https://doi.org/10.1115/PVP2006-ICPVT-11-93553.
7. Liu G L, Yang J X, Yang X W, et al. Influence of radial clearance on contact characteristics of cross shaft universal joint bearings. Bearings, 2018. 468(11): 38-42, http://dx.doi.org/10.19533/j.issn1000-3762.2018.11.010.
8. Liu J. A dynamic modelling method of a rotor-roller bearing-housing system with a localized fault including the additional excitation zone. Journal of Sound and Vibration, 2020, 469: 115144. https://doi.org/10.1016/j.jsv.2019.115144.
9. Liu J, Tang C, Pan G. Dynamic modeling and simulation of a flexible-rotor ball bearing system. Journal of Vibration and Control, 2021: 10775463211034347. https://doi.org/10.1177/10775463211034347.
10. Liu J, Xu Y, Pan G. A combined acoustic and dynamic model of a defective ball bearing. Journal of Sound and Vibration, 2021, 501: 116029. https://doi.org/10.1016/j.jsv.2021.116029.
11. Liu J, Xu Z. A simulation investigation of lubricating characteristics for a cylindrical roller bearing of a high-power gearbox. Tribology International, 2022, 167: 107373. https://doi.org/10.1016/j.triboint.2021.107373.
12. Lochan S, Mehmanparast A, Wintle J. A review of fatigue performance of bolted connections in offshore wind turbines. Procedia Structural

Integrity, 2019, 17: 276-283, https://doi.org/10.1016/j.prostr.2019.08.037.

13. Luan Y, Guan Z Q, Cheng G D, et al. A simplified nonlinear dynamic model for the analysis of pipe structures with bolted flange joints. Journal of Sound and Vibration, 2012, 331(2): 325-344, https://doi.org/10.1016/j.jsv.2011.09.002.

14. Lu J W, Wang G C, Chen H, et al. Dynamic analysis of cross shaft type universal joint with clearance. Journal of Mechanical Science and Technology, 2013, 27(11): 3201-3205, https://doi.org/10.1007/s12206-013-0842-z.

15. Ma X S, Yu Z F, Han Y. Research on Angular Output Velocity of a Drive Shaft with Double Cross Universal Joints. International Journal of Plant Engineering and Management, 2011, 16(02): 119-124, http://dx.doi.org/ 10.13434/j.cnki.1007-4546.2011.02.008.

16. Nazarko P, Ziemianski L. Force identification in bolts of flange connections for structural health monitoring and failure prevention. Procedia Structural Integrity, 2017, 5: 460-467, https://doi.org/10.1016/j.prostr.2017.07.142.

17. Qin Z, Han Q, Chu F. Bolt loosening at rotating joint interface and its influence on rotor dynamics. Engineering Failure Analysis, 2016, 59: 456-466, https://doi.org/10.1016/j.engfailanal.2015.11.002.

18. Rośkowicz M, Godzimirski J, Jasztal M, et al. Improvement of fatigue life of riveted joints in helicopter airframes. Eksploatacja i Niezawodnosc – Maintenance and Reliability 2021, 23(1): 165–175, http://dx.doi.org/10.17531/ein.2021.1.17.

19. Shi W B, Du J, Gong G W. Fatigue damage analysis of bolts connection between mainshaft and flange on wind turbine. Machinery Design and Manufacture, 2020. 350(4): 233-236, http://dx.doi.org/10.19356/j.cnki.1001-3997.2020.04.054.

20. Shi Z, Liu J, Li H, et al. Dynamic simulation of a planet roller bearing considering the cage bridge crack. Engineering Failure Analysis, 2022, 131: 105849. https://doi.org/10.1016/j.engfailanal.2021.105849.

21. Venugopal S, Hithesh K, Karikalan L. Modification and analysis on fatigue study in universal joint of an automobile vehicle. Materials Today: Proceedings, 2021, 37: 975-978, https://doi.org/10.1016/j.matpr.2020.06.184.

22. Weijtjens W, Stang A, Devriendt C, et al. Bolted ring flanges in offshore-wind support structures-in-situ validation of load-transfer behaviour. Journal of Constructional Steel Research, 2021, 176: 106361, https://doi.org/10.1016/j.jcsr.2020.106361.

23. Weiser T, Corves B. Deflection modeling of a manipulator for mechanical design. Mechanism and Machine Theory, 2019, 137: 172-187, https://doi.org/10.1016/j.mechmachtheory.2019.03.025.

24. Wu G, Niu B. Dynamic stability of a tripod parallel robotic wrist featuring continuous end-effector rotation used for drill point grinder. Mechanism and Machine Theory, 2018, 129: 36-50, https://doi.org/10.1016/j.mechmachtheory.2018.06.020.

25. Yongxu Hu, Jianhui Lin, Andy C T. Failure analysis of gearbox in CRH high-speed train. Engineering Failure Analysis, 2019, 105: 110-126, https://doi.org/10.1016/j.engfailanal.2019.06.099.

26. Yuan F, Guo P d, Lu Y Q. Bolt force prediction using simplified finite element model and back propagation neural networks. 2016 IEEE Information Technology, Networking, Electronic and Automation Control Conference. IEEE, 2016: 520-523, https://doi.org/10.1109/ITNEC.2016.7560415.

27. Zeng X H, Xu Y, Zhang Y, Xu Z H. Modeling of casing flange bolt connection and analysis of sealing performance. Advances in Aeronautical Science and Engineering. 2021, 12(2):143-149, https://doi.org/10.16615/j.cnki.1674-8190.2021.02.17.

28. Zhang G, Du J, To S. Study of the workspace of a class of universal joints. Mechanism and Machine Theory, 2014, 73: 244-258, https://doi.org/10.1016/j.mechmachtheory.2013.11.004.

29. Zhou Z, Yang L C, Liang Y, Zeng Y. Fracture analysis on high-strength flange bolts used in wind turbine foundation. Acta Energiae Solars Sinica, 2016, 37(9): 2230-2235, http://dx.doi.org/10.3969/j.issn.0254-0096.2016.09.009.